Refinement of atmospheric correction of absorbing aerosols for highly productive coastal waters using the SWIR retrieval algorithm together with water leaving reflectance constraints at 412nm

Marco Vargas, Min Oo, Alex Gilerson, Barry Gross, Fred Moshary, Sam Ahmed

Optical Remote Sensing Laboratory City College of New York, New York, NY, USA 10031

e-mail: gross@ccny.cuny.edu

Abstract: The recently developed SWIR atmospheric correction algorithm for ocean color retrieval uses long wavelength channels to retrieve atmospheric parameters to avoid bright pixel contamination. However, this retrieval is highly sensitive to errors in the aerosol model which is magnified by the higher variability of aerosols observed over urban coastal areas. While adding extra regional aerosol models into the retrieval Lookup Tables (LUT's) would tend to increase retrieval error since these models are hard to distinguish in the IR, we explore the possibility that for highly productive waters with high CDOM, an estimate of the 412nm channel water leaving reflectance can be used to constrain the aerosol model retrieval and improve the water leaving reflectance retrieval. Simulations show that this constraint is particularly useful where aerosol diversity is significant. To assess this algorithm, we compare our retrievals to the operational SeaDAS SWIR and NIR retrievals using insitu validation data in the Chesapeake Bay and show that especially for absorbing aerosols, significant improvement is obtained. Further insight is also obtained by intercomparison of retrieved Rrs images at 443nm and 551nm which demonstrates the removal of anomalous artifacts in the operational SeaDAS retrieval.

OCIS codes: 010.1110, 010.1690, 010.0280.

1) Introduction

Accurate retrieval of water leaving radiances from ocean color satellite observations, such as SeaWIFS or MODIS, requires accurate correction algorithms to compensate for atmospheric impacts. For open ocean conditions, an atmospheric correction scheme [1] was developed where the aerosol contribution was estimated using top of atmosphere (TOA) reflectances obtained from the SeaWIFS 765-865 (or MODIS 748-869) NIR channels under the reasonable assumption that the water leaving radiance at these wavelengths is negligible (black pixel approximation) due to strong water absorption. This atmospheric correction algorithm works well in open ocean waters, but tends to over correct for the atmosphere in coastal waters where the black pixel assumption is no longer valid[2-3] due to the increased reflection from hydrosol scattering. Thus, if the water leaving radiance is not negligible in the NIR bands, the retrieved aerosol loading will be overestimated resulting in underestimated or even negative water leaving radiances[4-5] for the 412nm channel.

To help compensate for these "bright" pixel contaminations, an attempt was made within the operational SeaWiFS Data Analysis System (SeaDAS) [6] to estimate the water leaving radiance in the NIR through the use of regression relations between the VIS water leaving radiances and the NIR water leaving radiances [7-9]. Such an estimate of the NIR water leaving radiances can then be used to arrive at a better aerosol path reflectance in the NIR channels and presumably lead to improved joint aerosol and ocean color retrievals. This method is equally suitable to MODIS and SeaWIFS but this approach obviously depends on the quality of the NIR regression relations which can significantly vary over diverse coastal waters.

To avoid these NIR algorithm difficulties, an approach [10] for atmospheric correction in coastal waters that uses different short wave infrared (SWIR) bands (i.e. MODIS 1240 and 2130nm) was proposed for operational retrieval of coastal water color and tested within SeaDAS. It should be pointed out that algorithms using the SWIR bands for atmospheric correction are not new and have been a staple of the hyperspectral imaging community including aircraft sensors such as AVIRIS and satellite sensors such as Hyperion [11-12]. This approach is based on the fact that ocean water absorbs strongly in this spectral region and the contributions of the in-water constituents are negligible and can safely be considered dark. However, at these long wavelengths, the atmospheric reflectance itself is significantly weaker and spectral features due to absorbing aerosols or fine urban modes are particularly difficult to resolve. Therefore, the retrieval error for water leaving radiances in the VIS channels using the SWIR bands is larger than that obtained using the NIR bands as long as the pixels in the NIR are sufficiently dark (or can be estimated with sufficient accuracy)

Based on these considerations, a constraint on the aerosol path reflectance in the visible is needed to improve retrievals, and in particular distinguish between oceanic, fine mode and absorbing aerosols. The purpose of this paper is to investigate the consequences of using the 412nm channel together with the SWIR retrieval algorithm to provide this constraint, and help distinguish and better quantify aerosols. We show that in the productive waters of the Chesapeake Bay, where the 412nm water leaving reflectance is reduced due to high Chlorophyll (ChL) and Color Dissolved Organic Matter (CDOM) absorption, significant improvement in atmospheric retrieval can be obtained resulting in improved water leaving reflectances. This paper is organized in 6 sections: following this introduction (section 1), in section 2 we explore the statistical variability of the 412nm water leaving reflectance using available SeaBASS measurements. From these datasets, we calculate the statistical distribution to determine the mean estimator as well as the error in the estimator for both 1σ and 2σ confidence levels. To assess the performance of the mean estimator, a quantitative comparison using a bio-optical model estimator approach [13] to provide a "bio-optical" constraint at 412nm is performed to determine the best estimator for coastal waters. In section 3, a radiative transfer model is presented and both the conventional NIR and SWIR atmospheric correction schemes are briefly described. In particular, we note that SeaDAS relies on historical oceanic phenomological models which do not properly account for absorbing[13] and fine mode aerosols which are fairly common for eastern US coastal environments. To include this variability, microphysical models based on NASA Aerosol Robotic Network (AERONET) aerosol retrievals from the Maryland Science Center, SERC and the COVE sites that are downwind from the Chesapeake Bay are used to generate radiative transfer LUT's which are combined with the SeaDAS models to provide more representative LUT's [14]. In section 4, sensitivity metrics are defined for measuring retrieval error over an ensemble of atmospheres and atmospheric retrieval sensitivity studies are presented for the traditional NIR retrieval approach. In section 5, we assess the aerosol retrieval and associated water leaving reflectance retrievals for both the NIR and SWIR correction scheme and show that the use of the "threshold" constraint introduced in section 2 for the 412 nm aerosol reflectance results in significant improvements in water leaving reflectance in the visible bands when the extended aerosol LUT's introduced in section 3 are used. In addition comparisons with in-situ remote sensing reflectance and aerosol optical depth are explored. Further comparisons are also made between Rrs retrieval images at 443nm and 551nm as well as AOD retrievals. In section 6, our conclusions are presented.

2) Choosing the 412nm normalized water leaving reflectance constraint

In our scheme, the 412nm channel TOA reflectance can help constrain the aerosol retrieval and provide compensation only if the normalized water leaving reflectance at 412nm is estimated a-priori with a reasonable accuracy, as the normalized water leaving reflectance uncertainty is the predominant factor in the error budget. For this to be the case, other factors which may contribute to the TOA signal uncertainty such as ozone and NO_2 are assumed to be corrected using concentration information obtained from UV profilers such as the OMI sensor on Aura [15-16] coupled to radiative transfer calculations for correction. In addition, it is well known [17] that at 412nm, errors using the scalar radiative transfer algorithm versus a vector radiative transfer algorithm can be as high as 3-5% of the total reflectance at TOA. However, we take the position that in future, a suitable processing based on the full vector radiative transfer code will replace the current atmospheric LUT's for both the SeaDAS and Aeronet atmospheres with out altering at least qualitatively our investigation

Two methods for estimating the $[\rho_{wn}(412)]$ parameter are considered. In the first approach, we can determine a best estimate by simply using the mean value obtained from large scale in-situ measurements. The statistics are based on SeaBASS database measurements in the Chesapeake region which are illustrated in figure 1. Unlike the deep water reflectances, we see that the normalized water leaving reflectance at 412nm $[\rho_{wn}(412)]$ is relatively low and stable which are consistent with high CDOM coastal waters in which the reflection is dramatically quenched, which is a necessary condition for the development of a relatively accurate estimator. To see if this approach is optimal, we contrast it with a bio-optical estimator approach which was introduced in [10] to correct for absorbing aerosols contamination by providing an estimate of 412nm water leaving reflectance. In this scheme, this is done by using normalized water leaving reflectances at longer wavelengths which are expected to be less affected by uncertainties in the aerosol modeling and compensation (i.e. Rrs_488, Rrs_551 and Rrs_678) and ingesting them into a bio-optical model which can then be extrapolated to provide an estimate of $\rho_{wn}(412)$. However, in testing this bio-optical estimator on the normalized water leaving reflectances in the SeaBASS database, we find the estimator generally underestimates the insitu value and this bias result in a larger uncertainty as seen in figure 2. To quantitatively compare these two approaches, we plot in figure 3 the cumulative distributions of the residual $\varepsilon = |\rho_{wn}(412) - est[\rho_{wn}(412)]|$ for the two estimators. We first note that the mean estimator significantly outperforms the "biased" bio-optical estimator for the Chesapeake region. However, on a global scale (deep water), the mean estimator is no longer useful and the bio-optical estimator can provide a better constraint, although both estimators perform poorly in comparison to the Chesapeake results. In addition, we also plot the residuals for the situation where the bio-optical estimator retrieval is modified to remove its bias by subtracting the mean of the residuals. While this is not a reasonable modification to the bio-optical estimator approach in practice, it does provide a lower limit to the uncertainty that can be achieved. In particular, we find that even when the bio-optical estimator is externally corrected for bias, the uncertainty in the threshold estimator is still optimal, especially beyond the 1σ confidence level. These observations clearly illustrate that the simple mean estimator is best suited to providing a constraint on the 412nm water leaving reflectance. Finally, from the cumulative distribution functions calculated in figure 3, we find that the uncertainty in the mean estimator can be quantified as:

$\rho_{wn} = \overline{\rho}_{wn} + \Delta\rho_{wn}$ where $\Delta\rho_{wn}^{1\sigma} = .003$ at (1σ) and $\Delta\rho_{wn}^{2\sigma} = .005$

3) Atmospheric correction

a) Background

The signal received at the TOA by an ocean color satellite sensor (i.e., SeaWIFS, MODIS) may be written as [9]

$$L_t(\lambda) = L_r(\lambda) + L_A(\lambda) + t_u(\lambda)L_{wc}(\lambda) + T_u(\lambda)L_g(\lambda) + t_u(\lambda)L_w(\lambda) \qquad (1)$$

where $L_r(\lambda), L_A(\lambda), L_{wc}(\lambda), L_g(\lambda)$ and $L_w(\lambda)$, are the contributions due to molecular scattering (Rayleigh), aerosol and Rayleigh-aerosol scattering (i.e. $L_A(\lambda) = L_a(\lambda) + L_{ra}(\lambda)$), whitecaps, sunglint, and ocean water respectively. Here, $T_u(\lambda)$ and $t_u(\lambda)$ are the direct and diffuse upwelling transmittances of the atmosphere.

The radiance L can be converted to reflectance ρ using the relation $\rho = \dfrac{\pi L}{F_0 \cos\theta_0}$ where F_0 is the extraterrestrial solar irradiance and θ_0 is the solar zenith angle. Assuming that the contributions from sunglint and whitecaps have been removed, equation (2) can be written as

$$\rho_A(\lambda) = \rho_t(\lambda) - \rho_r(\lambda) - t_u(\lambda)t_d(\lambda)\rho_{wn}(\lambda) \qquad (2)$$

where the conventional normalized water reflectance which is used to separate the atmospheric illumination affects from the reflection process, $\rho_{wn} = \rho_w / t_d$, has been adopted where t_d is the diffuse downwelling transmission.

For conventional atmospheric correction, both SeaWIFS and MODIS have bands in the NIR (i.e., 765/865 nm and 748/869 nm respectively) for which $\rho_{wn}(\lambda)$ is assumed zero. While this is normally valid in case I waters (Black Pixel Approximation), coastal waters with large sediment concentrations will often have significant water leaving signals at both NIR bands. This observation has led to the current approach in coastal waters of using the SWIR bands available for the MODIS sensor at 1240 and 2130 in which the black pixel assumption is valid under all reasonable conditions.

Historically, the inversions of the aerosols were done in a sequential fashion where the model was retrieved first and then the optical depth obtained second. In detail, defining λ_s and λ_l to represent the shorter and longer IR bands, the measured aerosol path reflectance spectral ratio (epsilon factor $\varepsilon^{MS}(\lambda_S, \lambda_l) = \rho_A(\lambda_S) / \rho_A(\lambda_l)$), which is fairly insensitive to aerosol optical depth at the TOA, is compared (within the black pixel approximation) with the epsilon values generated from within a pre-calculated look up table (LUT). By minimizing the error between measured and modeled ε factors, the appropriate aerosol model from the suite of aerosol models could be determined. Once the model is selected, the optical depth for that aerosol model can then be determined by equating the aerosol reflectance $\rho_{A,Mod}(\lambda_S, \tau)$ to the TOA reflectance. Once the aerosol model and optical depth at λ_S is determined, the atmospheric reflectance can be obtained from the LUT for all relevant wavelengths and the ocean reflectance $\rho_{wn}(\lambda)$ calculated from equation (4) for the visible bands. However, this approach becomes more inaccurate for SWIR where the extrapolation to the VIS is more problematic. In fact, it is no longer reasonable to use ε factors since the ratio of the aerosol path reflectances in log space are no longer linear over the increased spectral range. In fact it is necessary to apply a simultaneous fitting of the TOA reflectances to derive simultaneously the model and optical depth. This approach is the only one used in both the simulation and matchup data cases and is in fact quite similar to the spectral matching method of Gao et al [11-12]. Finally, we would like to emphasize that we will use the language of ε factors in subsequent sections but this is only to illustrate the need for aerosol LUT with more variability than available in SeaDAS and to reinforce the difficulties (including nonlinearity) in extrapolating from the SWIR to the VIS channels.

b) Aerosol Model Selection

In order to assess the uncertainty in the normalized water leaving reflectance inherent in the SWIR approach, as well as to assess the utility of the statistical estimates of $\rho_{wn}(412)$ in reducing the retrieval uncertainty, we need to calculate the appropriate LUT's based on an inclusive set of atmospheric models. At present, SeaDAS uses 12 aerosol models in the standard processing; these are the oceanic, maritime and tropospheric models which are based on the models developed by Shettle and Fenn[18] and an additional coastal aerosol model to represent the aerosol over the oceans near the coast was added by Gordon et al[16]. These aerosol models are the oceanic model with relative humidity of (RH= 99%) (denoted as O99), the maritime model with RH= 50%, 70%, 90% and 99% (denoted as M50, M70, M90, and M99), the coastal model with RH= 50%, 70%, 90% and 99% (denoted as C50, C70, C90, and C99), and the tropospheric model with RH= 50%, 90% and 99% (denoted as T50, T90, and T99). This suite of aerosol models is used to generate the aerosol LUT's and represents mostly nonabsorbing and weakly absorbing aerosols.

To illustrate the variability of the SeaDAS aerosol models, figures 4 a,b show the spectral variation of the epsilon function relevant for the NIR correction and SWIR correction $\varepsilon(\lambda,869) \equiv \rho_{aer}(\lambda)/\rho_{aer}(869)$; $\varepsilon(\lambda,2130) \equiv \rho_{aer}(\lambda)/\rho_{aer}(2130)$ which illustrates the spectral behavior of the aerosol path reflectance for both the NIR and SWIR correction schemes. A solar zenith angle of 60^{o}, a sensor zenith angle of 45^{o}, and a relative azimuth angle of 90^{o} were used

to maximize the atmospheric perturbations and to avoid sun-glint:

Unlike the SeaDAS approach for estimating atmospheres over water using climatological models, the MODIS retrieval of aerosol properties is governed by Aeronet based models. In the conventional scheme, a set of fine and coarse models are obtained through a cluster based analysis [19] and the retrieval is based on linear mixing of the finer and coarse modes. One approach to develop a reasonable LUT based on this scheme would be to use a linear mixture of all possible modes with a wide variety of mixing ratios to build up the LUT's. However, it is much more representative to build up the LUT based on existing atmospheric Aeronet retrievals over a specific geographic region. In particular, since we are looking specifically at the Chesapeake bay, we use a combination of MD Science Center, COVE and SERC data obtained from 2005-2006.

While the SeaDAS LUT's we used were obtained directly from the source code, the Aeronet atmospheric aerosol models were generated by us with the SHARM radiative transfer code [20]. In building the LUT, the historical approach is to use one dimension for the aerosol model and another dimension for the optical depth. However, as discussed previously, we choose to merge both the aerosol model and optical depth which results in 159 phase functions (aerosol models) and 10 different AOD levels (i.e. 1590 atmospheres) as described in Table 1. From this set, we can then use multichannel TOA measurements (as well as a-priori estimates of water leaving reflectance at 412nm) to constrain the aerosol model and optical depth simultaneously. In particular, by matching all constraints simultaneously, we can obtain a list of joint models and optical depths $\{M_j, \tau_j\}$ which are consistent with all spectral channel constraints. From this list, we may obtain the statistics of aerosol retrieval including mean and standard deviation etc. The details of this approach are given in section 4.

To see how the aerosol models compare, we plot in figure 5a,b the epsilon factors $\log[\varepsilon(\lambda,2130)]$ for both SeaDAS and AERONET based atmospheres. In particular, a large number of high angstrom coefficient aerosol models $1 \le \log[\varepsilon_{aeronet}(412,2130)] \le 3.5$ are observed in AERONET which are not included in the SeaDAS LUT's $0 \le \log[\varepsilon_{SeaDAS}(412,2130)] \le 2.5$. While the different domains for the ε parameters show a need for a modified LUT, the effect of absorbing aerosols whose affects are increased in the blue (due to enhanced rayleigh-aerosol interaction) are obscured. To see the absorbing aerosol effects more clearly, we plot in figure 6 the relationship between the path reflectance (blue/green) ratio $\Delta = \rho_{aer}(412)/\rho_{aer}(555)$ as it relates to the aerosol single scatter albedo ω_0. Clearly, a strong monotonic behavior is seen between the albedo and the blue/green ratio which if not included in the LUT, will lead to unphysical retrievals. However, the spread in the spectral ratio around the best fit (quadratic) line does not show a significantly larger data spread as the single scattering albedo is reduced. This suggests that this set can describe the absorbing aerosol properties quite well and the concerns of aerosol vertical structure is reduced due to the natural stability in how aerosols are distributed vertically for a given region. Of course, the existence of high altitude absorbing aerosol plumes will dramatically alter this approach and would require real time input from an active lidar system such as the Micropulse

Lidar. To further demonstrate that the SeaDAS models do not provide the needed variability, we plot in figure 7 the cumulative distribution function for Δ over the aeronet atmospheres which are compared to the SeaDAS model values. We note a small percentage (5%) of atmospheres (absorbing) have blue green ratios below the smallest SeaDAS based ratio and as much as 20% of the aeronet atmospheres have values above the largest

To account for the natural variability of aerosols, it would be nice to be able to combine the complementary LUT's using a-priori statistics to weight the likelihood of each individual element. However, the data needed to obtain such a true weighting is limited by the restrictions placed on the AERONET retrieval which result in retrievals biased to high angstrom coefficient, making it impractical to assign relative weights to elements in the LUT. Instead, we will focus on a worst case scenario where the weights of the LUT elements are taken to be equal. It is our purpose to show that even in this extreme case, where the uncertainties in the retrieval are expected to be at their maximum, the constraint imposed at 412nm on the upwelling water radiance for the Chesapeake is sufficient to reduce the retrieval errors to values that would be comparable to those obtained solely based on the restricted SeaDAS LUT. This suggests an algorithm which can perform retrievals over a more diverse LUT including both fine mode and absorbing aerosols that can increase the percentage of retrievals while keeping the errors constrained to those obtained

4) Water Leaving Reflectance Error Metrics

Once the appropriate LUT's are constructed, we can assess the retrieval errors for the normalized water reflectance which occur due to the uncertainties in the atmospheric model determination. In this work, the main contributor to the uncertainty seen on the VIS channels can be ascribed to the aerosol model retrieval since we assume that a suitable assimilation of auxiliary measurements of total path ozone and NO_2 [16,21] will reduce gaseous transmittance and gas-aerosol uncertainties.

Based on the radiative transfer model formulation given in eqn (2), the retrieval error for water leaving reflectance will depend on the variability of the atmospheric parameters ρ_a, $\left(t^2 = t_d t_u\right)$, the channel noise as well as the mean value of the normalized water leaving reflectance. The details of the procedure are as follows

Step #1: Find all possible LUT atmospheres (enumerated by index i) in which the atmosphere path reflectance data for all atmospheric channels is consistent with the TOA reflectance and all other constraints are satisfied. Since the study is synthetic, we define the "true" signal to be the TOA signal for atmosphere model (k). Mathematically, we construct the atmosphere set S_k to satisfy all the following constraints simultaneously. The formulations of the constraints are divided into radiometric constraints and water leaving constraints. In the radiometric case, the constraints are based on receiver specifications while the water leaving constraints are based on estimates of normalized water leaving reflectances ρ_{wn} and the estimator uncertainty $\Delta\rho_{wn}$. These constraints will be applied by us to assess both the conventional bright pixel contamination in the NIR channels or in the 412nm channel.

Dark Pixel (Radiometric) channel constraints:

$$\begin{aligned} & i \in S_k \quad iff \left\| \rho_{i,aer}^{LUT}(\lambda_l) - \rho_k^{\mathrm{TOA}}(\lambda_l) \right\| = \left\| \rho_{i,aer}^{LUT}(\lambda_l) - \rho_{k,aer}^{\mathrm{LUT}}(\lambda_l) \right\| \leq NE\Delta\rho_l \\ & l = \text{all } \textit{atmospheric} \text{ spectral bands} \end{aligned} \tag{3a}$$

where $NE\Delta\rho_l$ is the Noise Equivalent Path Reflectance for channel (l)

(Water leaving Reflectance) Constraint:

$$i \in S_k \quad iff \left\| \frac{\rho_i(\lambda_l) - \rho_k(\lambda_l)}{t_{d,k}(\lambda_l) t_{d,k}(\lambda_l)} + \left[\bar{\rho}_{wn}\right]_l \left[\frac{t_{d,i}(\lambda_l) t_{d,i}(\lambda_l)}{t_{d,k}(\lambda_l) t_{d,k}(\lambda_l)} - 1 \right] \right\| \leq \left[\Delta\rho_{wn}\right]_l \tag{3b}$$

Satisfying the appropriate constraints simultaneously results in the determination of the set S_k which contains all possible retrieval atmospheres for the reference atmosphere (k).

Step #2: For each atmospheric model (i) in the resultant ensemble set S_k, calculate the normalized water leaving reflectance as $[\rho_{wn}]_i = \dfrac{\rho_t - [\rho_{atm}]_i}{[t_d t_u]_i}$

Step #3: Once all the water signals are calculated, we perform an average $[\rho_{wn}]_{ret}^k = \langle [\rho_{wn}]_i \rangle$

Step #4 Finally, we average (for convenience) over all atmospheres to obtain the LUT averaged retrieval $[\rho_{wn}]_{ret} = \langle [\rho_{wn}]_{ret}^k \rangle$

5) Algorithm Intercomparison Studies

5.1 Long wavelength Constraints

To begin our sensitivity analysis, the radiometric sensitivities of the MODIS channels must be specified. The MODIS noise equivalent radiances $(NE\Delta L)$ were taken from IOCCG report [22] These radiances were converted to noise equivalent reflectance using $NE\Delta\rho = \dfrac{\pi \times NE\Delta L}{F_0 Cos(\theta_0)}$, where F_0 is the solar extraterrestrial irradiance. Their values are given in Table 2.

These noise levels are calculated for the individual pixel but in accordance to the aerosol retrieval algorithms for MODIS [23] the SWIR channels are first aggregated into 10km x 10km boxes which pass through a series of filters for removal of clouds, glint etc. The final retrieval requires that number of quality pixels $N_p > 30$ which we set as our standard. Therefore, all per pixel $NE\Delta\rho$ values are reduced by the square root of the pixel number

$$[NE\Delta\rho]_{eff} = NE\Delta\rho \Big/ \sqrt{N_p} \qquad (4)$$

5.2 NIR algorithm with water leaving estimator.

Before evaluating sensitivities for SWIR algorithms, it is useful to revisit the traditional NIR atmospheric correction scheme. In the standard operating procedure for coastal waters, the dark pixel approximation is no longer used ; instead a NIR estimator based on normalized water leaving reflectance in the VIS (and ChL estimates) is used to predict the NIR normalized water leaving reflectance. [24]

To assess the accuracy of this estimator, we use public domain data based on hydrolight simulations generated by Lee et al[25] of water leaving reflectance suitable for coastal water conditions as part of the IOCCG report. In figure 8, we plot the fractional error in the estimator relative to the measured value (as obtained from the IOCCG database) for $\rho_{wn}(760)$ and observe that the error in the estimator (at the 1σ level) is about 10%. These results are similar to the 865nm estimator although the error is slightly higher. . With this assessment of the errors that occur when NIR estimators are used to estimate the water leaving reflectance in the NIR channels, we can define the error in the NIR atmospheric channels as

$$NE\Delta\rho(\lambda_{NIR}) = f\,\overline{\rho_{wn}(\lambda_{NIR})} \qquad (5)$$

where the mean normalized water leaving reflectance obtained from the SeaBASS database is used and f is the bright pixel compensation factor. For example, $f = 1$ corresponds to no attempt at correcting for bright pixels, $f = 0.1$ corresponds to an estimate of the bright pixel to 10% accuracy and $f = 0.01$ corresponds to a level of bright pixel compensation to the 1% level.

The results for the NIR atmospheric retrieval case are presented in figure 9 as a statistical cumulative distribution function of fractional normalized water leaving reflectance uncertainties in the visible wavelengths (relevant to ChL retrieval) over the set of all possible atmospheres in the atmospheric LUT. These illustrate that for the limited SeaDAS atmospheric LUT, at the 1σ level, errors of $\Delta\rho_{wn}(443) \approx 30\%, \Delta\rho_{wn}(488) \approx 15\%,$ and $\Delta\rho_{wn}(551) \approx 5\%$ are found. However, the same calculation based on the cumulative (SeaDAS + Aeronet) LUT results in much higher errors of $\Delta\rho_{wn}(443) \approx 120\%, \Delta\rho_{wn}(488) \approx 50\%, \Delta\rho_{wn}(551) \approx 10\%$. In particular, we note the error in the 443 channel is much too large when used as input into ChL algorithms currently employed. [26]

5.3 SWIR algorithm with additional 412nm water leaving constraint

For the SWIR correction scheme [(1240,2130)], we first examine the retrieval uncertainty using the SeaDAS LUT. The results are shown in figure 10 where the constraint on the 412nm channel is varied. In particular, we consider the case where no constraint at 412nm is used, the application of the constraint $\rho_{wn}^{1\sigma}(412) = \overline{\rho}_{wn} \pm .003$ which is the $1\sigma \approx (60\%)$ confidence level and the 2σ confidence level constraint $\rho_{wn}^{2\sigma}(412) = \overline{\rho}_{wn} \pm .005$. The results show that for the limited SeaDAS LUT, the effect of the 412nm constraint is minimal. However, it is interesting to note that the errors using the SWIR are approximately $\Delta\rho_{wn}(443) \approx 20\%, \Delta\rho_{wn}(488) \approx 10\%,$ and $\Delta\rho_{wn}(551) \approx 3\%$ which is ~ 50% improvement over the NIR approach, showing the usefulness of the SWIR approach in general.

To summarize, table 3 shows the results of the uncertainty in the normalized water leaving reflectance for the 443, 488 and 551 nm bands for the NIR and SWIR algorithm for both the SeaDAS and (SeaDAS+Aeronet) LUT's, and how they are improved when the constraint at 412nm is used. The results can be summarized as follows

1. The retrieval error from conventional NIR algorithm becomes extremely significant if the level of bright pixel contamination compensation is less than 90% (f=.1) The errors are even more severe when the combined Aeronet – SeaDAS LUT is used.

2. In comparison to the NIR algorithm with realistic bright pixel compensation errors, the unconstrained SWIR algorithm retrieval error is ~ 25% less. This result is also approximately true when employing the combined Aeronet – SeaDAS LUT.

3. When the combined SeaDAS + Aeronet tables are used, the 412nm constraint is much more important as seen in figure 11. Without the 412 constraint, the errors at 443nm become very large due to the added spectral variability of the atmospheric models. The weaker 2σ confidence level constraint helps reduce the errors to some extent but with the stronger 1σ constraint, the errors in the water leaving retrievals are commensurate with the results using the SeaDAS LUT alone.

5.4 Assessment of 412 constraint algorithm on insitu data sets

5.4.1 Matchup Comparisons

To summarize, we have proposed a modification based on sensitivity studies of the operational SeaDAS SWIR algorithm by increasing the number of aerosol models to account for local aerosol climatology as well as using in-situ derived statistical constraints of the normalized water leaving reflectance at 412nm to provide an added restriction on the selection of the final aerosol model. As pointed out earlier, this approach works best for notable CDOM absorption that reduces the 412nm water signal and is therefore particularly useful in the Chesapeake where moderate to high levels of CDOM is often observed. In particular, without this strict constraint, the retrieval error within the SWIR approach would be much higher when more extensive aerosol model LUT's based on regional observations are used.

To assess our approach more directly, we first compare in-situ normalized water leaving reflectances obtained from insitu measurements from the NOMAD database with those obtained from our retrieval method as well as those obtained using the operational SeaDAS SWIR algorithm as applied to MODIS AQUA measurements. Our focus during the inter-comparison is the 443 nm channel since this channel is the most difficult for retrieval (besides the 412nm channel) and the channel most positively affected by the 412nm constraint. Table 4 lists the location sites in the Chesapeake as well as the results of our comparison. Here, in-situ data of upwelling radiance and downwelling irradiance stored in the NOMAD database are used to compute the insitu Rrs values. These matchup cases were chosen because of the availability of aerosol optical depth retrievals from AERONET, insitu remote sensing reflectance, as well as AOD and remote sensing reflectance retrievals using the standard SWIR algorithm of SeaDAS.

To begin, we examine the aerosol optical depth retrievals. The results of the AOD comparison are given in figure 12 for the operational SWIR using the 16 SeaDAS aerosol models and our current constrained algorithm using the regional models. In particular, we see that both algorithms seem to provide a reasonable estimate of the AOD although the modified algorithm seems to show the best improvement in the retrieval when AOD is relatively small. Error bars are provided in the modified algorithm based on the standard deviation of AOD retrievals that satisfy all SWIR radiometric constraints as well as the 412 water leaving constraint. The reason for the improved AOD is more clearly illustrated in figure 13 where the AOD match-ups are compared to the aerosol single scatter albedo (SSA). In particular, the SeaDAS models clearly overestimate the aerosol AOD when the SSA < 0.9 illustrating the benefits of including more regional absorbing aerosol models.

Finally, we compare in figure 14, the remote sensing reflectance obtained from our algorithm with the standard SWIR model as well as the NIR algorithm (when possible) Although neither retrieval approach seems completely satisfactory, we do note the removal of negative retrievals in our approach which occur in the standard processing due to the presence of a moderately absorbing aerosol modes discussed above. This undesirable feature is also seen when the NIR algorithm is used. On the other hand, we also see significant improvement using our constrained regional algorithm retrieval to insitu data for matchup sites 11-17 in comparison to the SWIR algorithm. These matchups occur in the coastal ocean outside the Chesapeake Bay area (the blue sites in figure 15) where the NIR algorithm is expected to be superior to the SWIR which is indeed the case. However, while it is expected that the NIR algorithm should perform better than the SWIR outside the bay, the magnitude of the discrepancy is quite remarkable. This can be explained by noting that the aerosol reflection ratio $\rho_{aer}(412)/\rho_{aer}(555)$ for these matchups has a mean value of 1.32 which is outside the range within the SeaDAS models.(see fig 7) Therefore, within the SeaDAS retrieval, the 412 aerosol reflectance is likely to be underestimated resulting in an overestimate of the water signal. This mechanism together with the significant extrapolation errors inherent in the SWIR algorithm from an inaccurate optical depth aerosol model can clearly lead to dramatic errors when trying to retrieve water leaving signals which are quite small due to ChL and CDOM absorption. However, even under these difficult retrieval conditions, the 412nm constraints seem to be sufficient to improve the retrieval to the level of the NIR algorithm.

5.4.2 Image Comparison

Optimally, spatial comparison of our algorithm to the current SeaDAS retrievals would require us to directly assimilate into the SeaDAS processing stream the selection algorithm for of the best atmospheric model based on regional aerosol models and constraint approach outlined above. However, preliminary comparisons are presented here based on a limited emulation of the SeaDAS processing but substituting our atmospheric selection algorithm.. In particular, to avoid differences in pre-processing, we use the Level 2 SeaDAS outputs directly to generate the TOA reflectances in the VIS and NIR. Unfortunately, the SeaDAS TOA reflectance is not generated for the SWIR bands at 1240 and 2130, so we must process these directly from the MODIS Level 1B reflectances. As a preliminary consistency check, and to ensure that no significant errors due to possible differences in the pre-processing occur, we compare in figure 16, the TOA reflectance at 869nm which were calculated from both SeaDAS and our processing of the MODIS Level 1B data. Cursory inspection of the matchup shows good agreement and supporting statistical analysis shows that errors over all points < 2% with a one standard deviation level of about 0.5%.

For comparison purposes, we present an illustrative cloud-free case (Oct 3 2003) which has the added feature that much of the SeaDAS retrieved Rrs at 443nm is anomalously negative.

The most interesting comparisons between SeaDAS SWIR retrievals of the remote sensing reflectance for 443nm and 551 nm and our regionally constrained approach are made in fig 17. We first note (panel b) the dramatic anomalous negative Rrs at 443 nm from SeaDAS together with the fact that that the effect is dramatically stratified between the west (negative) and east (positive) shorelines. The constrained regional retrieval on the other hand removes the anomalous negative Rrs values and the unphysical stratification seems to be significantly removed. The results at 551nm are less dramatic since the effects of aerosol diversity is less pronounced and the overall water leaving signal in most cases is significantly larger than at 443nm.

However, it is important to point out that our constrained regional retrieval does not find a suitable solution in all cases where SeaDAS retrieval was successful. In particular, the narrow western tributaries as well as a gap near the center of the bay were unsuitable for retrieval. In examining these regions, looking at the TOA reflectances (figure 16), it is clear that retrievals would be grossly inaccurate since these regions have anomalous bright reflectance patches due to either inadequate cloud mask or in the case of the tributaries, to possible ground reflectance contamination from the surrounding shore. The fact that these questionable regions are being processed by SeaDAS is evident in dramatic anomalies in the retrieved Rrs values as well as the aerosol optical depth as seen in fig 18. Interestingly, we note the same east-west stratification in the retrieved AOD retrieval which is again eliminated in our approach. In fact, the overestimation of AOD for the western bank seems to be highly correlated to the underestimation of the Rrs.

6) Conclusions

To avoid the bright pixel contamination in the traditional NIR bands of MODIS, a SWIR algorithm was introduced within the SeaDAS development environment. However, the current operational algorithm uses a limited set of 12 ocean based aerosol models which do not address the complete variability of aerosol optical properties, especially in coastal region and in the vicinity urban/industrial areas. This can lead to poor retrieval results when exposed to aerosols models which have significantly different spectral features as observed in regional Aeronet retrievals. Such cases include highly absorbing aerosols whose effective TOA reflectance in the blue is relatively low, as well as urban non-absorbing aerosols with relatively high reflectance in the blue, and which cannot be easily distinguished with IR estimates alone. Clearly, if the increased diversity of aerosol spectral responses in the coastal zone is included within the atmospheric

LUT's used in the atmospheric correction procedure, a significantly larger retrieval error will occur unless additional constraints are used to restrict the set of aerosols for a given TOA signal.

In this paper, we have shown that if no additional constraints are added, the SWIR algorithm retrieval using the more realistic LUT will lead to unacceptable errors but that these errors can be removed if strong statistical constraints on the normalized water leaving reflectance at 412nm can be applied. In fact, we find that for the Chesapeake Bay, the high CDOM absorption lead to a quasi-black pixel condition which provides us with the tight constraints needed to retrieve water leaving reflectance using the more complete and regionally tuned atmospheric LUT. including fine mode aerosols and absorbing aerosols. This effectively translates into a higher percentage of successful retrievals for coastal environments.

In addition, we considered the possibility that a bio-optical estimator approach might provide a tighter constraint on the water leaving reflectance at 412nm. However, we found that errors in the bio-optical model are in fact significantly larger than the errors associated with the simple statistical estimator approach we have been considering. This is in part due to the bias inherent in the bio-optical estimator which makes it so useful in flagging high absorbing aerosol features but results in large quantitative errors

The testing of the algorithm against MODIS data sets was explored in section 5.4 where both AOD retrievals and remote sensing reflectance were considered. To summarize our observations in subsection 5.4.1, where retrievals were compared to insitu and ground based data, the constrained regional SWIR algorithm appears to provide a modest improvement on the AOD retrievals relative to AERONET retrievals. This is particularly the case when absorbing aerosols are considered. In fact, we find in this case that an overestimate in the aerosol optical depth in the traditional SWIR algorithm is significantly improved using the regional approach. In addition, when remote sensing reflectance at 443nm is considered, we find that both the NIR and SWIR algorithms still yield negative values which are corrected with our regional constrained approach. Even outside the Chesapeake, where the traditional SWIR algorithm performance is expected to be less accurate than traditional NIR algorithms, the constrained regional algorithm seems to perform at about the same level as the NIR algorithm in support of our numerical sensitivity studies. Further assessment of our approach was provided in 5.4.2 where retrieved images of Rrs at 443nm and 551nm as well as AOD at 551nm are compared for standard SeaDAS processing and SeaDAS processing augmented with our atmospheric selection algorithm. In particular, we note that the SeaDAS Rrs image had notable anomalous values which are eliminated in the constrained retrieval as expected for an algorithm which forces a positive reflectance at 412nm. More interestingly, the anomalous negative behavior of the SeaDAS retrieval seemed to be spatially stratified into west (negative) and east (positive) coast regions which is unlikely and a manifestation of a similar stratification seen in the AOD retrieval .On the other hand, agreement in the Rrs 551 retrieval matchup demonstrates the general soundness of our approach .

Finally, to study the approach in a more operational manner, more cases and regions need be explored and the choice of representative aerosol models must be reduced. At present, we are working at integrating our changes directly into SeaDAS.

Acknowledgements

This work is partially supported under grant NOAA #NA17AE1625

References:

[1] Gordon, H. R. and M. Wang. , “Retrieval of water-leaving radiance and aerosol optical thickness over the oceans with SeaWiFS: A preliminary algorithm”. Applied Optics, **33**, 443–452. (1994)

[2] Darecki, M., and D. Stramski. “An evaluation of MODIS and SeaWiFS bio-optical algorithms in the Baltic Sea”. *Remote Sensing of Environment*, 89, 326-350. (2004)

[3] K. G. Ruddick, F. Ovidio, and M. Rijkeboer, "Atmospheric Correction of SeaWiFS Imagery for Turbid Coastal and Inland Waters ," Appl. Opt. 39, 897-912 (2000)

[4] Lavender, S. J., Pinkerton, M. H., Moore, G. F., Aiken, J. & Blondeau-Patissier, D. "Modification to the atmospheric correction of SeaWiFS ocean colour images over turbid waters", Continental Shelf Research, 25, 539-555, 2005.

[5] Hu Chuanmin, Carder Kendall L, Muller Karger, Frank E. Atomospheric Correction of SeaWiFS Imagery over Turbid Coastal Waters: A practical method. Remote sensing of Environment, , 74, 195-206. (2000)

[6] http://oceancolor.gsfc.nasa.gov/seadas/

[7] Stumpf, R. P., R. A. Arnone, R. W. Gould, P. M. Martinolich, and V. Ransibrahmanakul (2003), A Partially Coupled Ocean-Atmosphere Model for Retrieval of Water-Leaving Radiance From SeaWiFS in Coastal Waters, SeaWiFS Postlaunch Tech. Rep. Ser., vol. 22, NASA Tech. Memo. 2003-206892, edited by S. B. Hooker and E. R. Firestone, pp. 51– 59, NASA Goddard Space Flight Cent., Greenbelt, Md.

[8] Arnone, R. A., P. Martinolich, R. W. Gould Jr., R. Stumpf, and S. Ladner, "Coastal optical properties using SeaWiFS," *Proceedings*, *Ocean Optics XIV*, S. Ackleson and J. Campbell (eds.), Office of Naval Research, Washington, DC,1998.

[9] D. A. Siegel, M. Wang, S. Maritorena, and W. Robinson, "Atmospheric Correction of Satellite Ocean Color Imagery: The Black Pixel Assumption ," Appl. Opt. 39, 3582-3591 (2000)

[10] M. Wang and W. Shi "Estimation of ocean contribution at the MODIS near-infrared wavelengths along the east coast of the U.S.: Two case studies" Geophys. Res. Lett, **32**, L13606, doi:10.1029/2005GL022917, (2005)

[11] Gao, B.-C., M. J. Montes, Z. Ahmad, and C. O. Davis, Atmospheric correction algorithm for hyperspectral remote sensing of ocean color from space, Appl. Opt., 39, 887-896, February 2000.

[12] Gao, B.-C., M. J. Montes, R.-R. Li, H. M. Dierssen, and C. O. Davis, An atmospheric correction algorithm for remote sensing of bright coastal waters using MODIS land and ocean channels in the solar spectral region, IEEE Tran. Geosc. Remote Sensing, 45, No. 6, 1835-1843, 2007 (doi:10.1109/TGRS.2007.895949).

[13], V. Ransibrahmanakul and R. P. Stumpf, 'Correcting ocean colour reflectance for absorbing aerosols", International Journal of Remote Sensing , 27, 1759 - 1774 , 2006

[14], R. C. Levy,_ L. A. Remer, J. V. Martins, and Y. J. Kaufman," Evaluation of the MODIS Aerosol Retrievals over Ocean and Land during CLAMS", *J. Atmos. Sci.,* **62,** 974–992. (2005)

[15] F. Levelt, E.Hilsenrath, G. W. L. Gijsbertus H. J. van den Oord, P.N. K. Bhartia, J.Tamminen, J. F. de Haan, and J. P. Veefkind, "Science Objectives of the Ozone

Monitoring Instrument”, *IEEE Transactions Geoscience and Rem. Sens.* **44**, 1199-1208 (2006)

[16] Ahmad, Z., McClain, C. R, Herman, J.R, Franz, B. A., Kwiatkowska, E., Robinson, W. D., Bucsela, E. D. and Tzortziou, M. ”Atmospheric correction for NO(2) absorption in retrieving water-leaving reflectances from the SeaWiFS and MODIS measurements”, Appl Opt 46 (26): 6504-12 (2007)

[17] Mishchenko, M. I., L. Travis, and A. Lacis, *Multiple Scattering of Light by Particles*, Cambridge University Press, Cambridge, 478 pp Chapter 13 sect. 1 (2006)

[18] Shettle, E. P., and R. W. Fenn (1979), Models for the aerosols of the lower atmosphere and the effects of humidity variations on their optical properties, Rep. AFGL-TR-79-0214, U.S. Air Force Geophys. Lab., Hanscom AFB, Mass.

[19] Omar, A. H., J. G. Won, et al. "Development of global aerosol models using cluster analysis of Aerosol Robotic Networrk (AERONET) measurements." JGR-Atmos. **110** (2005)

[20] A. I. Lyapustin, "Radiative transfer code SHARM for atmospheric and terrestrial applications," Appl. Opt. 44, 7764-7772 (2005)

[21] Earth Probe Total Ozone Mapping Spectrometer (TOMS) Data Products User's Guide. NASA Technical Publication 1998-206895.
ftp://toms.gsfc.nasa.gov/pub/eptoms/EARTHPROBE_USERGUIDE.PDF

[22] IOCCG Report Number 1. (1998). Minimum requirements for an operational ocean-colour sensor for the open ocean. Canada’ Dartmouth, p.46.

[23] L A. Remer, D. Tanre and Y. Kaufman, “Algorithm For Remote Sensing Of Tropospheric Aerosol From Modis: Collection 5” ATBD-02 Document http://modis.gsfc.nasa.gov/data/atbd/atbd_mod02.pdf

[24] J. A. Warrick, L. A. K. Mertes, D. A. Siegel and and C. Mackenzie, “Estimating suspended sediment concentrations in turbid coastal waters of the Santa Barbara Channel with SeaWiFS”, Int. J. Remote Sensing, **25** 1995–2002 (2004)

[25] Z. P. Lee, http://www.ioccg.org/groups/OCAG_data.html.

[26] O’Reilly, J.E., S. Maritorena, B.G. Mitchell, D.A. Siegel, K.L. Carder, S.A. Garver M. Kahru, and C.R. McClain, Ocean color chloro-phyll algorithms for SeaWiFS, J. Geophys. Res., **103**: 24,937-24,953, (1998).

Captions

Figure 1 Normalized water leaving reflectance insitu measurements from SeaBASS database

Figure.2 Intercomparison of measurements to bio-optical estimator to verify the property that the estimator in general underestimates the water leaving signal.

Figure 3 Cumulative distribution of residual error for both the bio-optical estimator and the mean (threshold) estimator. Both Chesapeake Bay and global waters are given.

Figure 4 Variability of Aerosol multiple scattering (log) epsilon (SeaDAS models) a) NIR b) SWIR

Figure 5 SWIR epsilon factors $\log(\varepsilon(\lambda,2130))$ for different atmosphere models a) SeaDAS LUT b) . Aeronet LUT

Figure 6. Relationship between albedo and atmosphere path reflectance (blue/green) ratio as function of aerosol single scattering albedo.

Figure 7. CDF for blue/green atmosphere ratio for aeronet site near Chesapeake.

Figure 8. Fractional error of 760nm estimator using data from SeaBASS database

Figure 9 Statistical cumulative distribution function of fractional normalized water leaving reflectance uncertainties using the NIR retrieval algorithm on the SeaDAS aerosol model LUT with different bright pixel compensation levels a) 443nm b) 488nm c) 551nm

Figure 10 Statistical cumulative distribution function of fractional normalized water leaving reflectance uncertainties using the SWIR retrieval algorithm on the SeaDAS with different 412nm water leaving reflectance constraint levels a) 443nm b) 488nm c) 551nm

Figure 11 Statistical cumulative distribution function of fractional normalized water leaving reflectance uncertainties using the SWIR retrieval algorithm on the SEADAS plus AERONET LUT with different 412nm water leaving reflectance constraint levels a) 443nm b) 488nm c) 551nm

Fig. 12 AOD retrieval a) SWIR using SeaDAS models and b) SWIR with regional models and 412nm constraint.

Fig. 13 Assessment of AOD retrieval for matchup data sets. a) SWIR using SeaDAS models compared to regional model b) Single Scatter Albedo for matchup cases

Fig. 14 Comparison of insitu measurements of normalized water leaving reflectance of SWIR retrieval using standard processing and regional model.

Fig. 15 Mapping of insitu matchups : red is non absorbing cases in bay (1-4), green is absorbing cases in bay (5-10) , blue is nonabsorbing outside bay (11-17). Numbering taken from table 4

Fig. 16 Intercomparison of TOA Reflectance at 869nm to ensure preprocessing of the SWIR bands is in agreement with SeaDAS a) SeaDAS b) MODIS DAAC + Processing

Fig. 17. Rrs reflectance comparisons a) constrained retrieval at 443nm b) SeaDAS retrieval at 443nm c) constrained retrieval at 551nm d) SeaDAS retrieval at 551nm

Fig. 18. Aerosol Optical Depth comparisons at 551 nm a) constrained retrieval b) SeaDAS retrieval

Table 1 Parameters and ranges used In Radiative Transfer LUT

Table 2 MODIS Noise Equivalent Delta Reflectance NE$\Delta\rho$ for a solar angle of 60 degrees

Table 3 Fractional Normalized water leaving reflectance uncertainties

Table 4 Matchups of insitu Remote Sensing Reflectance and SeaDAS retrievals including NIR and SWIR methods.

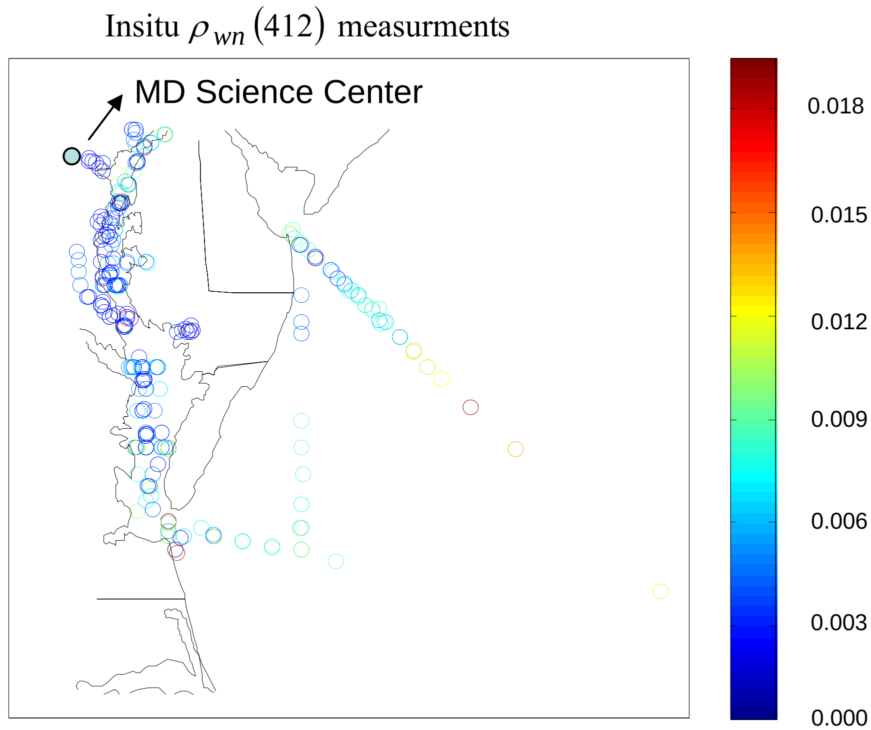

Fig. 1 Normalized water leaving reflectance insitu measurments from SeaBASS database.

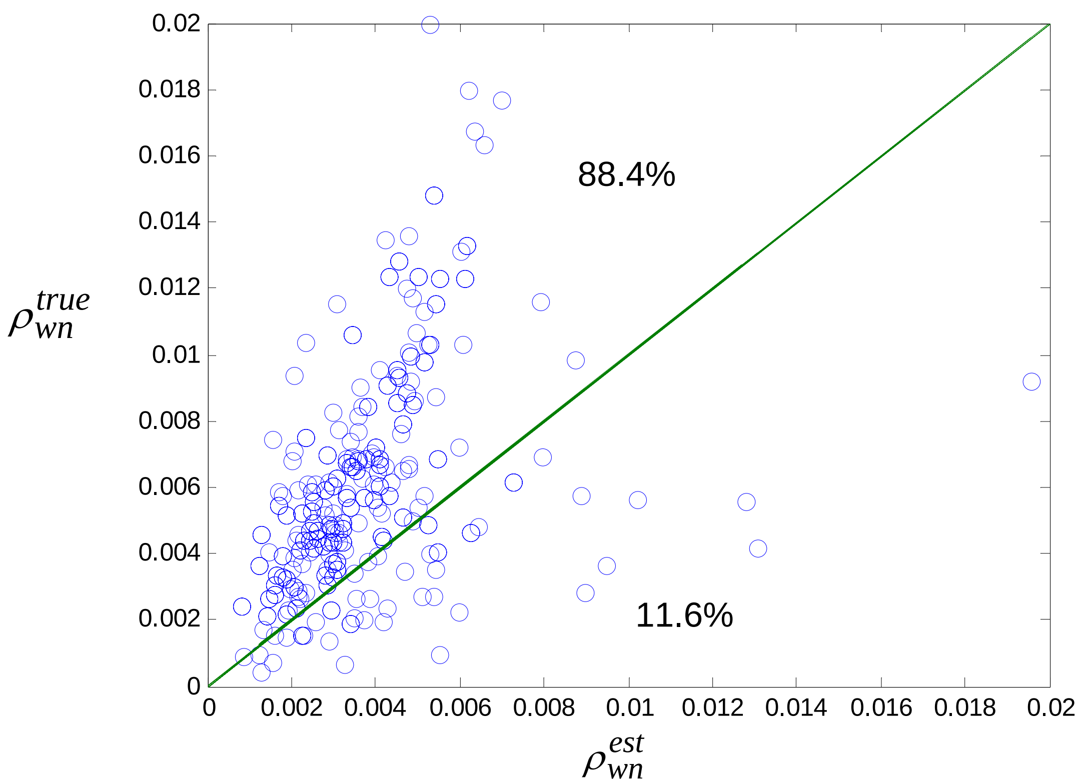

Fig.2 Intercomparison of measurements to bio-optical estimator to verify the property that the estimator in general underestimates the water leaving signal.

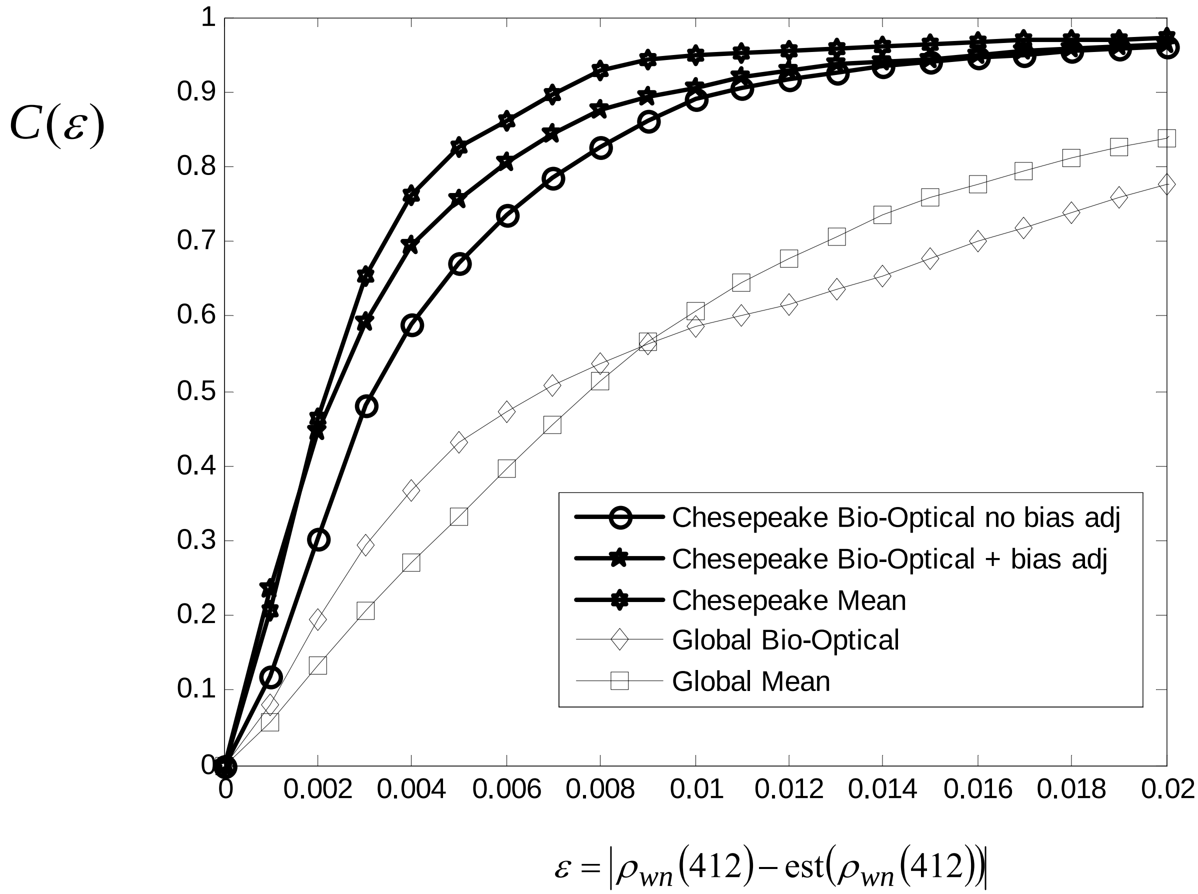

Fig. 3 Cumulative distribution of residual error for both the bio-optical estimator and the mean (threshold) estimator. Both Chesapake Bay and global waters are given.

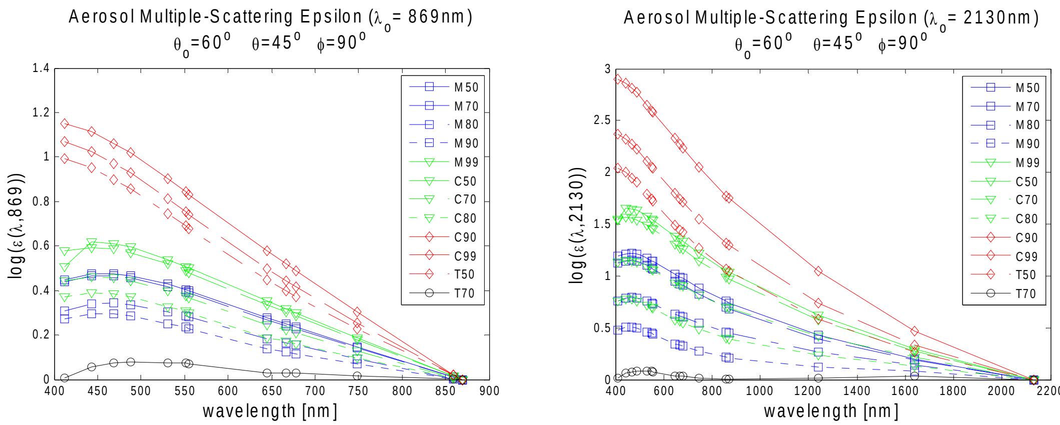

Figure 4 Variability of Aerosol multiple scattering (log) epsilon (SeaDAS models) a) NIR b) SWIR

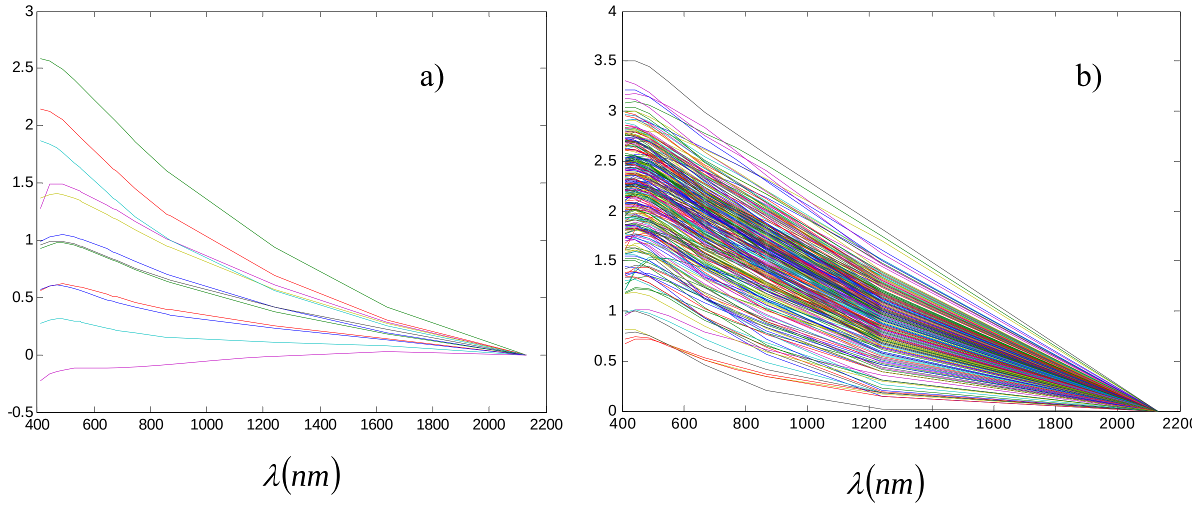

Figure 5 SWIR epsilon factors $\log(\varepsilon(\lambda,2130))$ for different atmosphere models a) SeaDAS LUT b) . Aeronet LUT

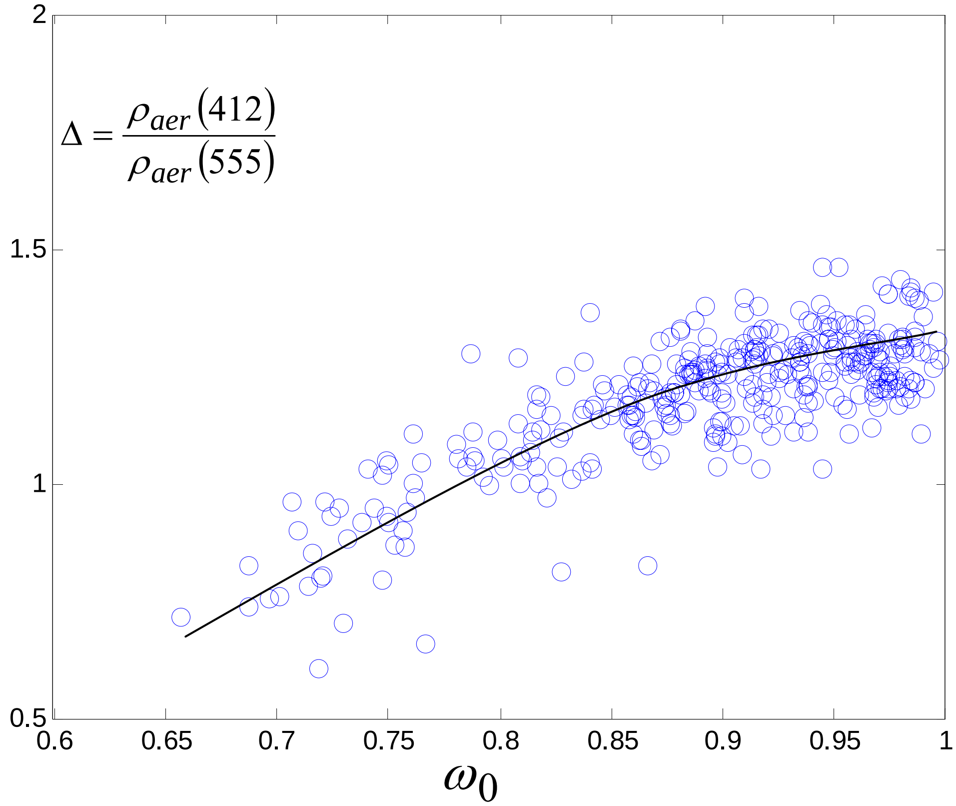

Figure 6. Relationship between albedo and atmosphere path reflectance (blue/green) ratio as function of aerosol single scattering albedo.

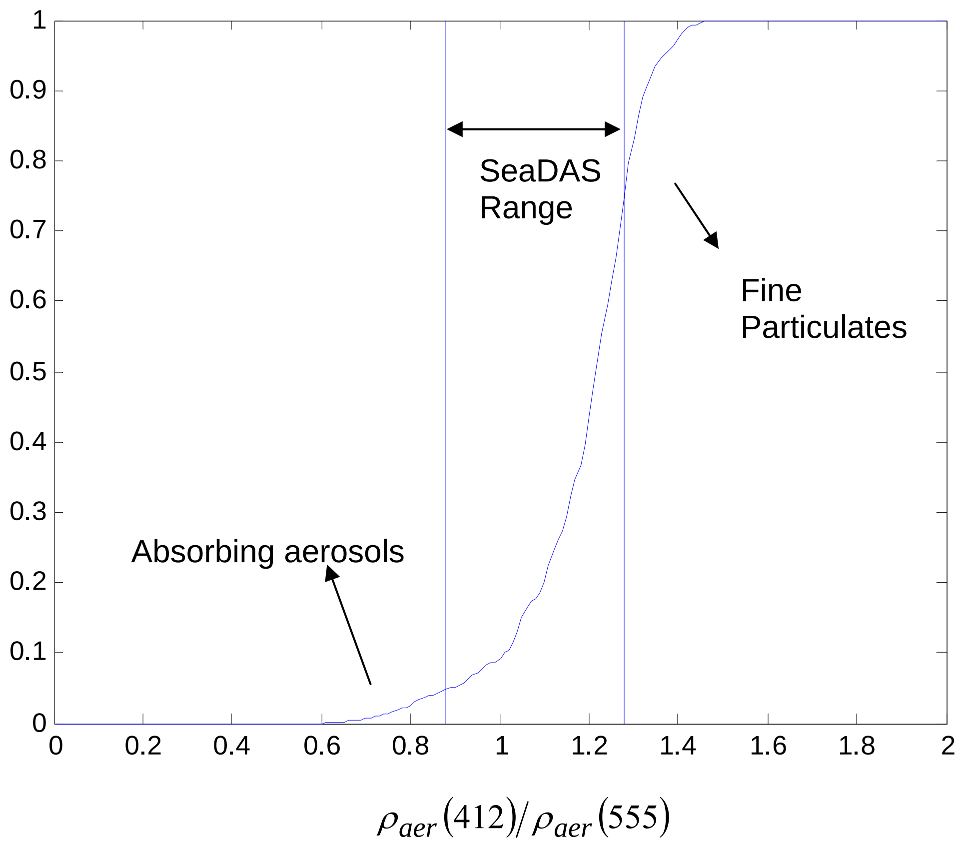

Figure 7. CDF for blue/green atmosphere ratio for aeronet site near chesepeake.

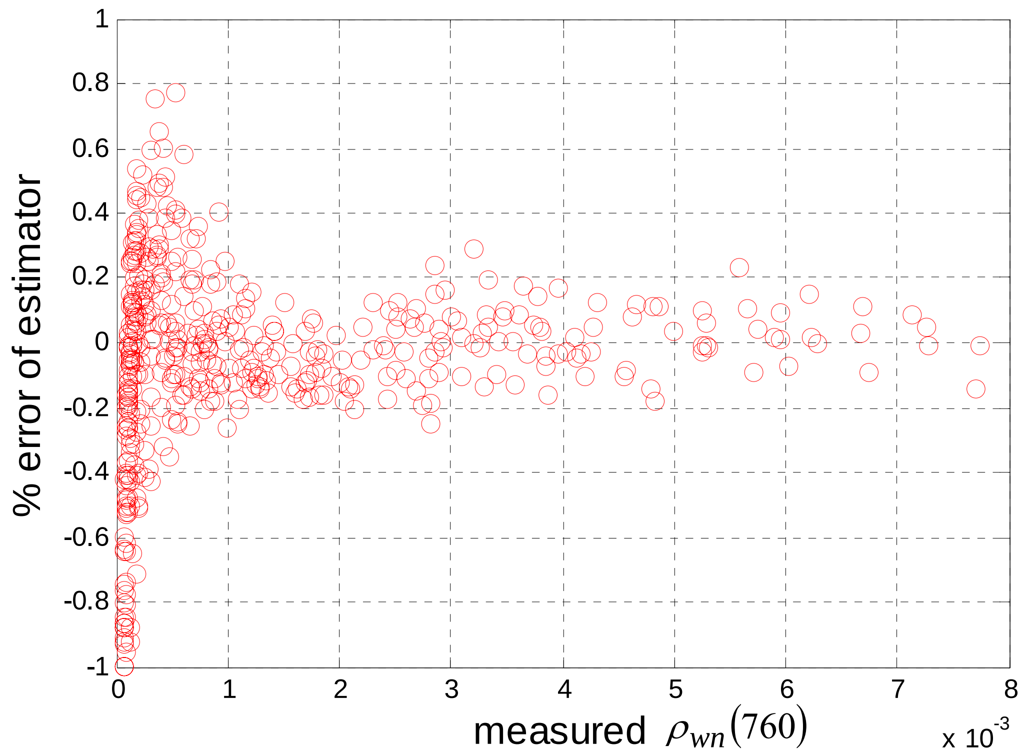

Figure 8. Fractional error of 760nm estimator using data from SeaBASS database

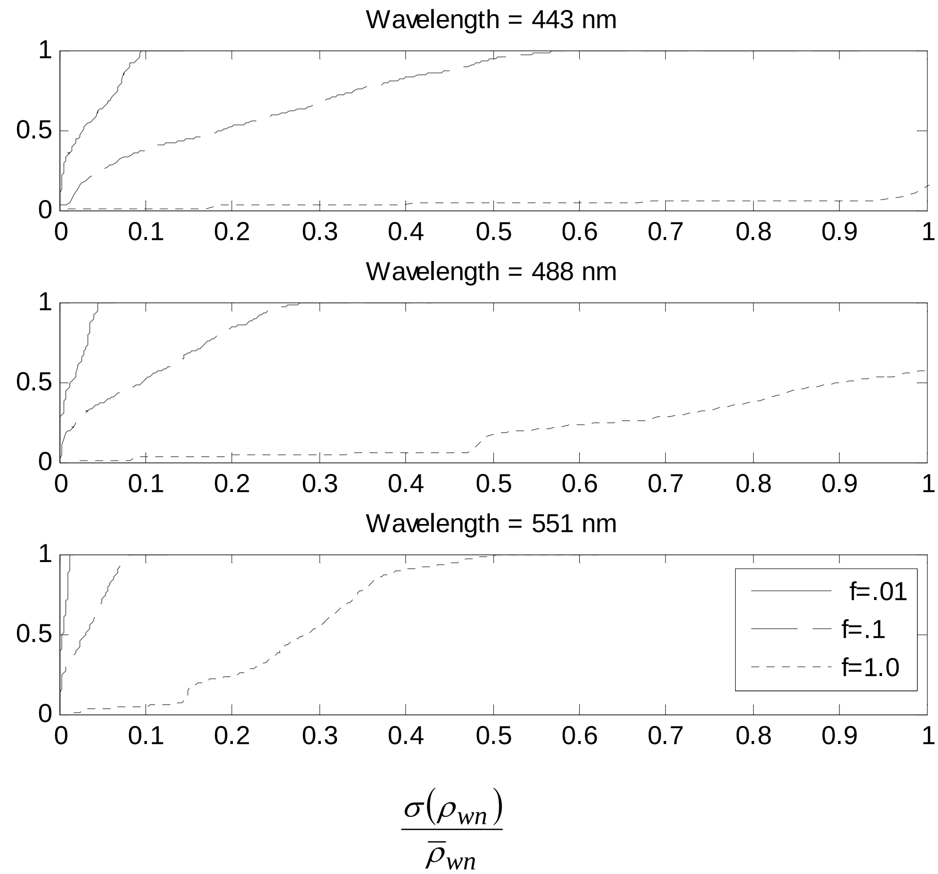

Figure 9 Statistical cumulative distribution function of fractional normalized water leaving reflectance uncertainties using the NIR retrieval algorithm with the SeaDAS aerosol model LUT’s with different bright pixel compensation levels a) 443nm b) 488nm c) 551nm

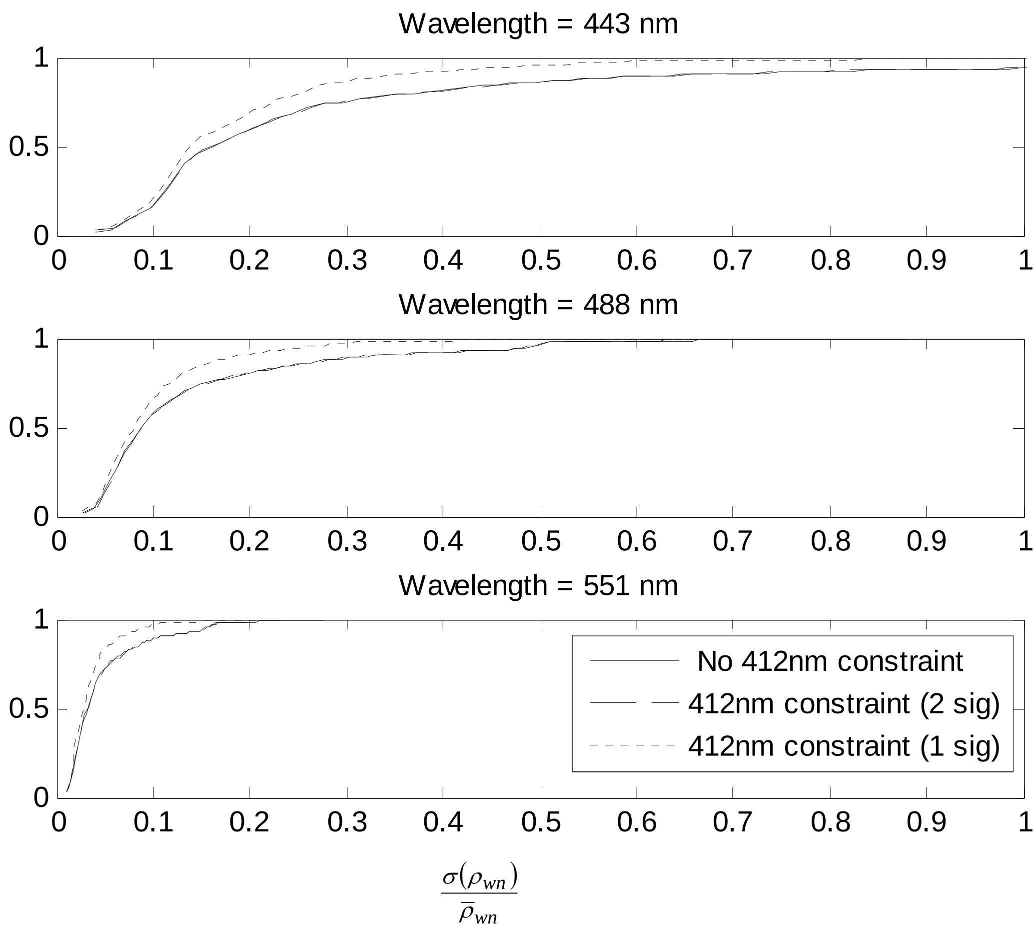

Figure 10 Statistical cumulative distribution function of fractional normalized water leaving reflectance uncertainties using the SWIR retrieval algorithm on the SeaDAS with different 412nm water leaving reflectance constraint levels a) 443nm b) 488nm c) 551nm

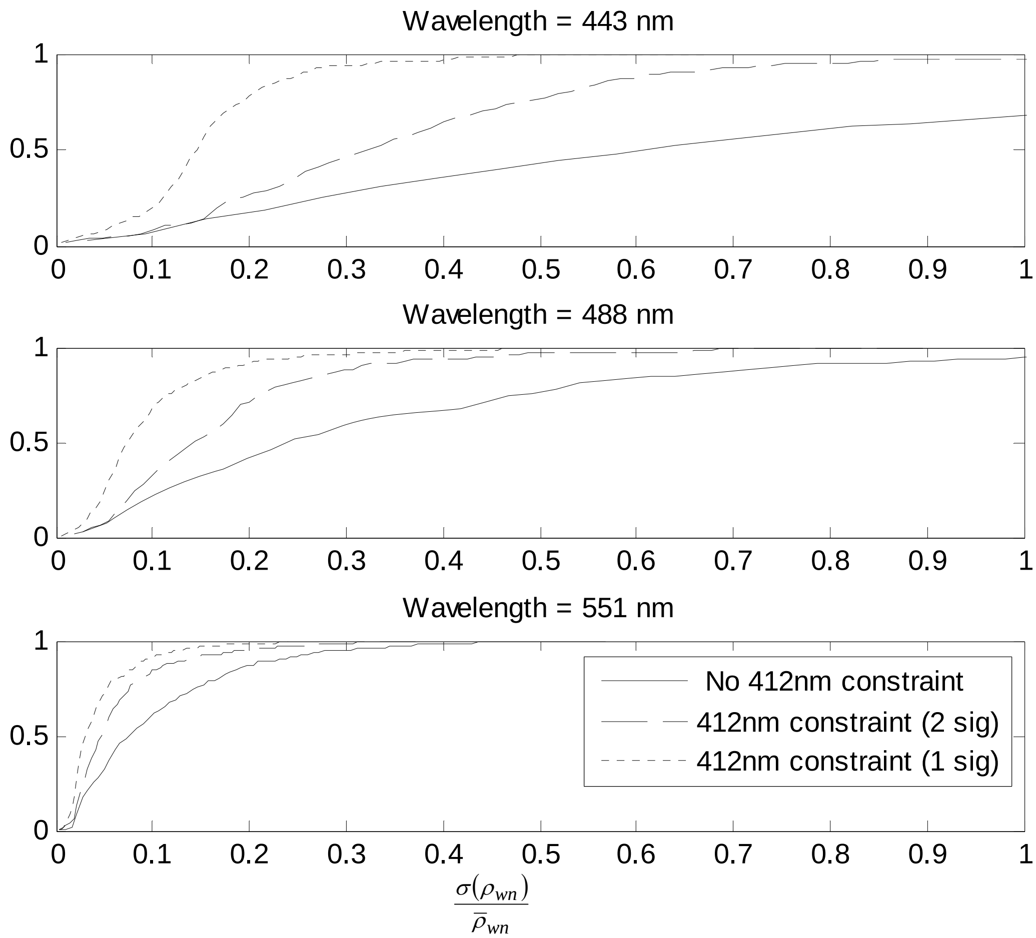

Figure 11 Statistical cumulative distribution function of fractional normalized water leaving reflectance uncertainties using the SWIR retrieval algorithm on the SEADAS plus AERONET LUT with different 412nm water leaving reflectance constraint levels a) 443nm b) 488nm c) 551nm

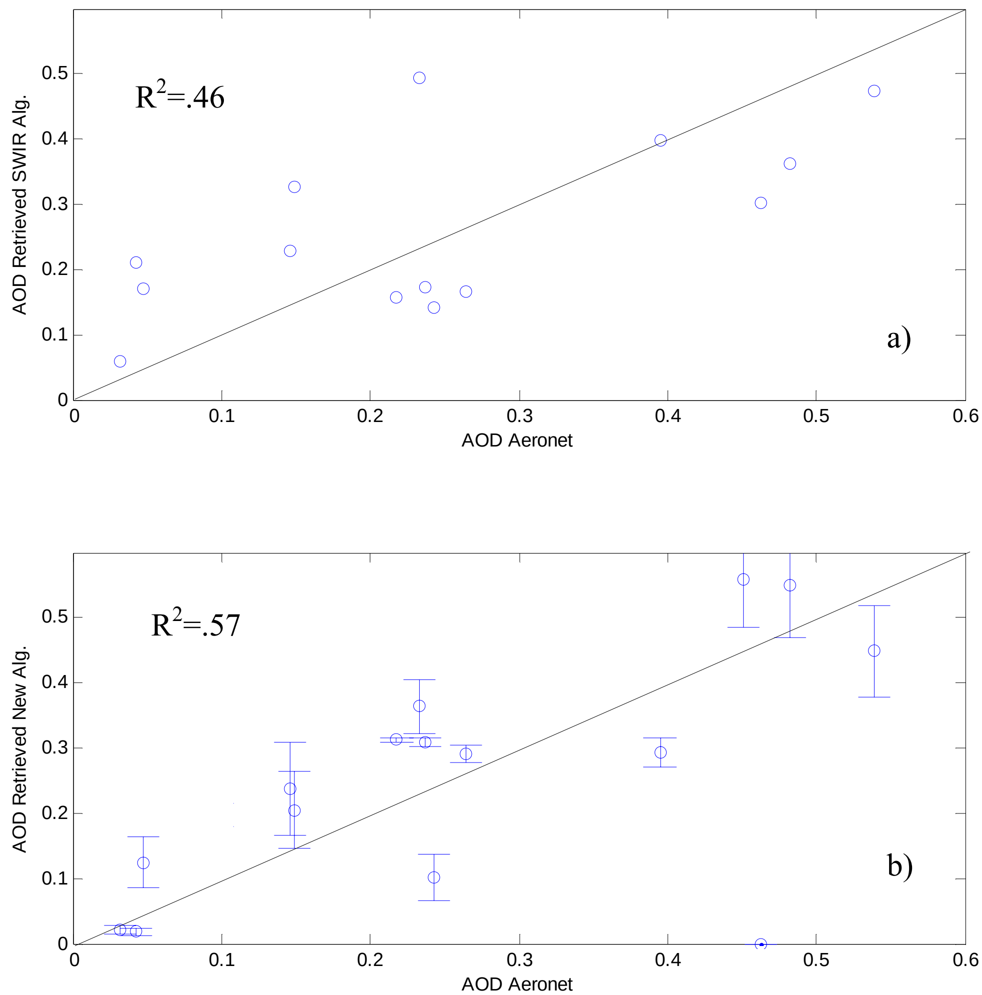

Fig. 12 AOD retrieval a) SWIR using SeaDAS models and b) SWIR with regional models and 412nm constraint.

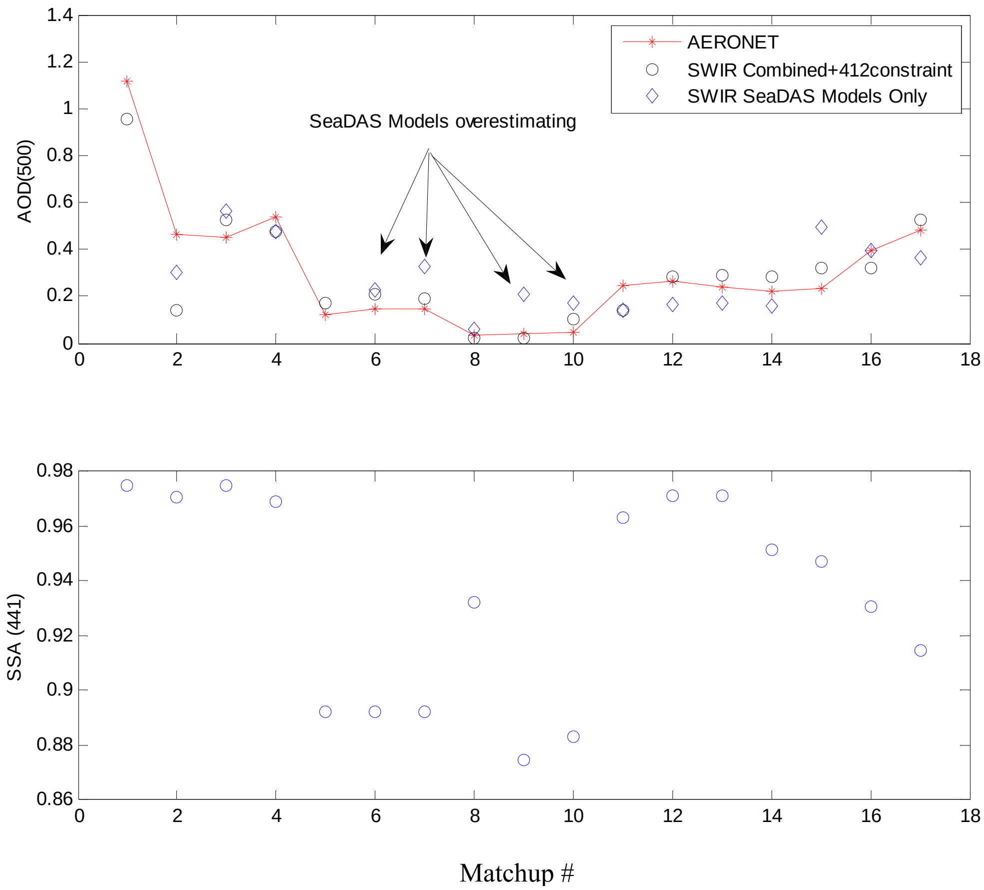

Fig. 13 Assessment of AOD retrieval for matchup data sets. a) SWIR using SeaDAS models compared to regional model b) Single Scatter Albedo for matchup cases

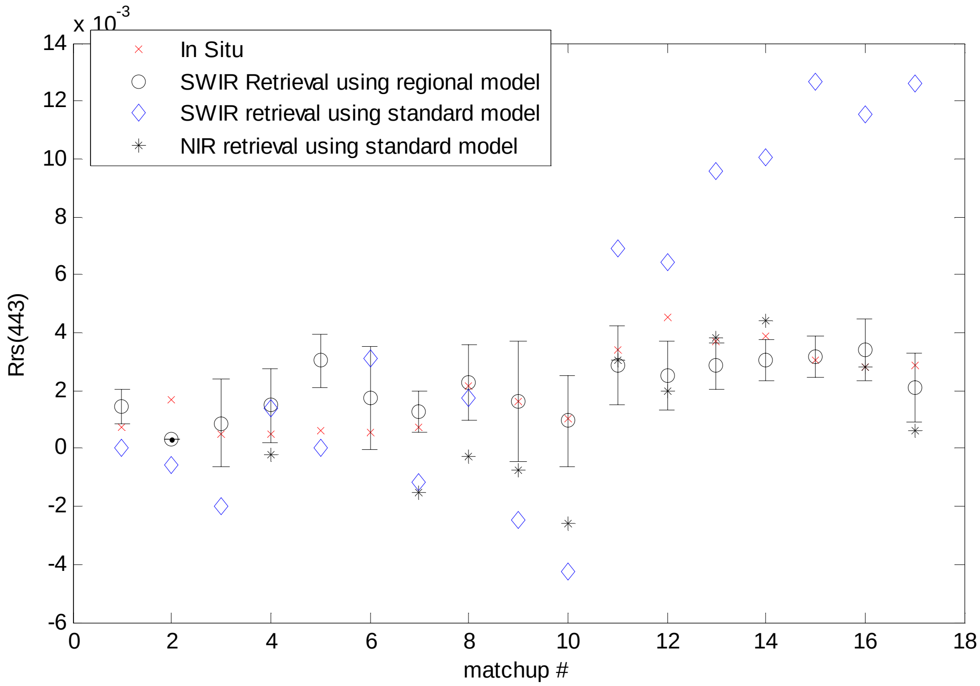

Fig. 14 Comparison of insitu measurements of normalized water leaving reflectance of SWIR retrieval using standard processing and regional model.

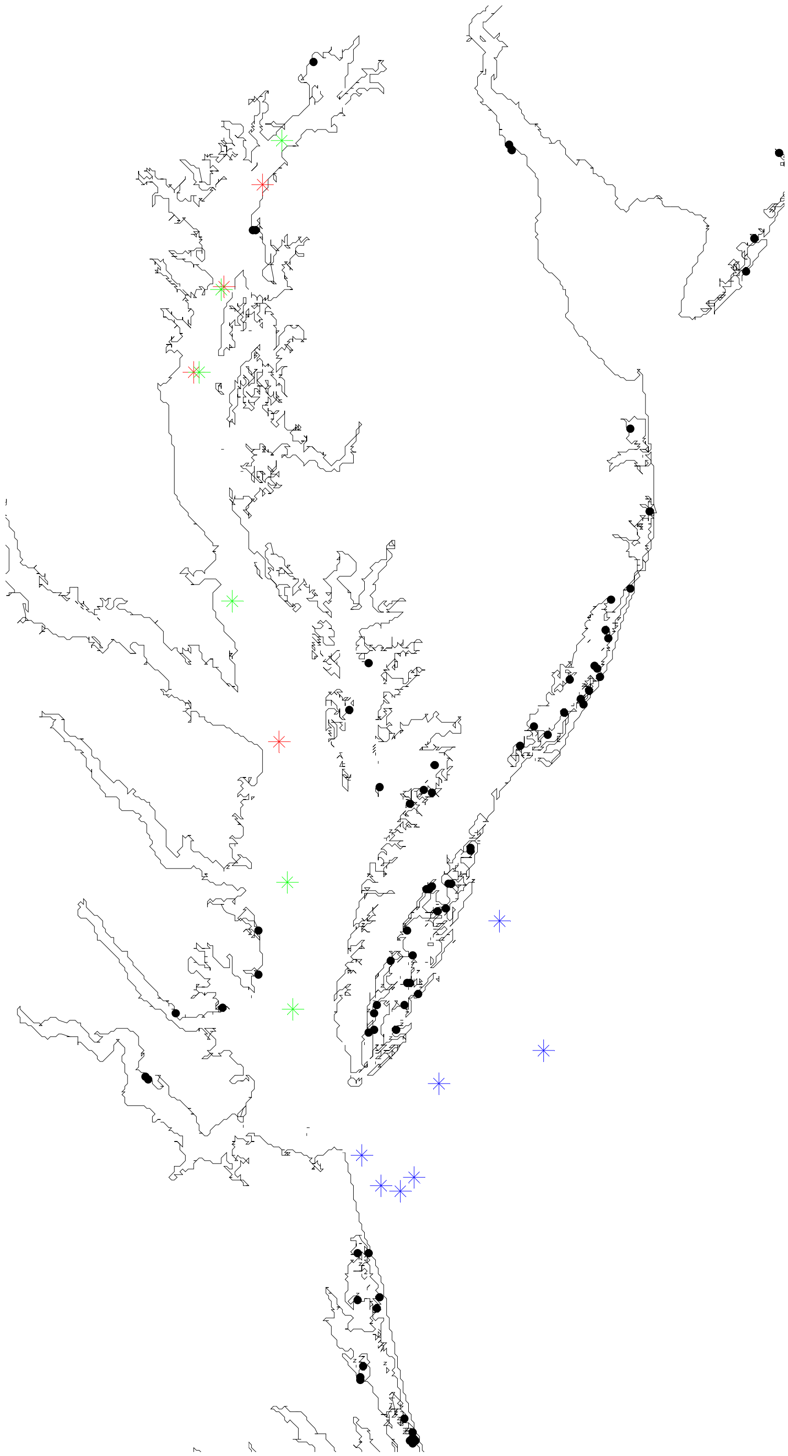

Fig. 15 Mapping of insitu matchups : red is non absorbing cases in bay (1-4), green is absorbing cases in bay (5-10) , blue is non-absorbing cases outside bay (11-17). Numbering taken from table 4

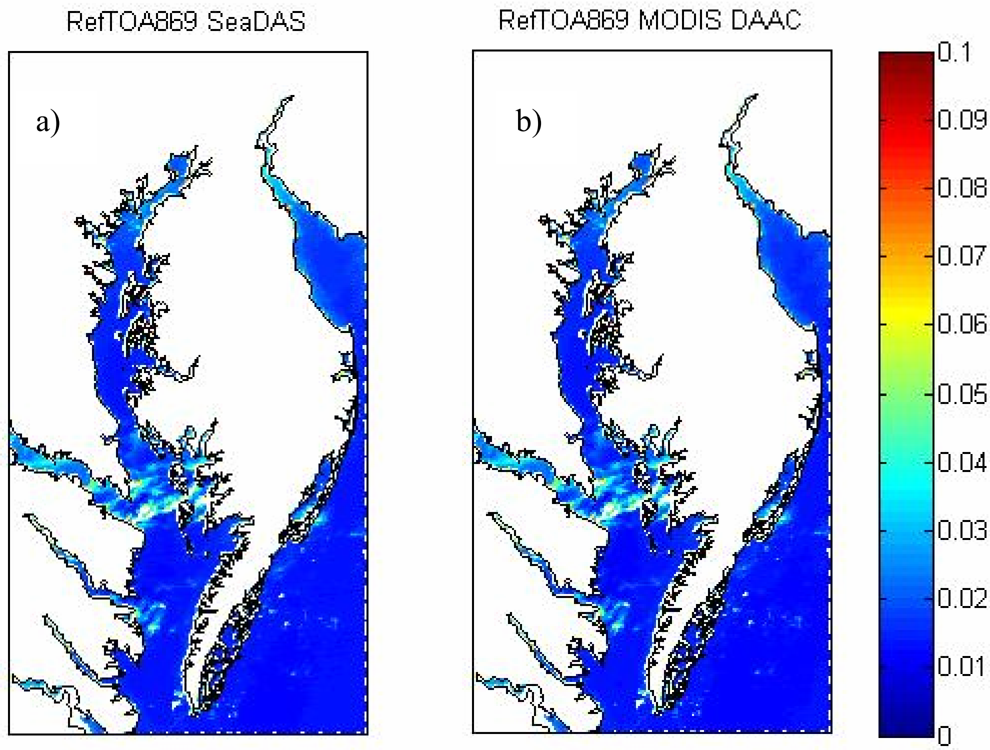

Fig. 16 Intercomparison of TOA Reflectance at 869nm to ensure preprocessing of the SWIR bands is in agreement with SeaDAS a) SeaDAS b) MODIS DAAC + Processing

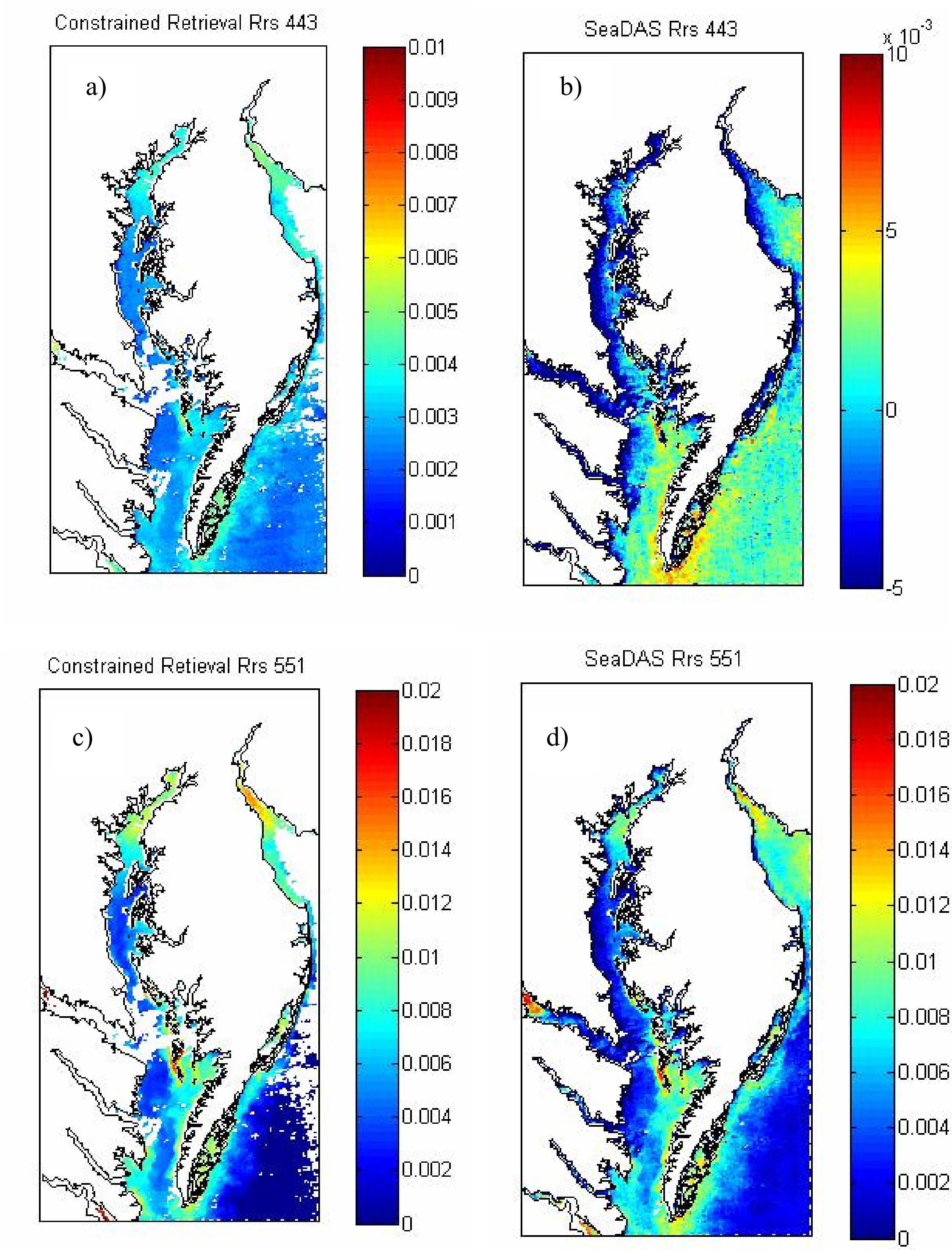

Fig. 17. Rrs reflectance comparisons a) constrained retrieval at 443nm b) SeaDAS retrieval at 443nm c) constrained retrieval at 551nm d) SeaDAS retrieval at 551nm

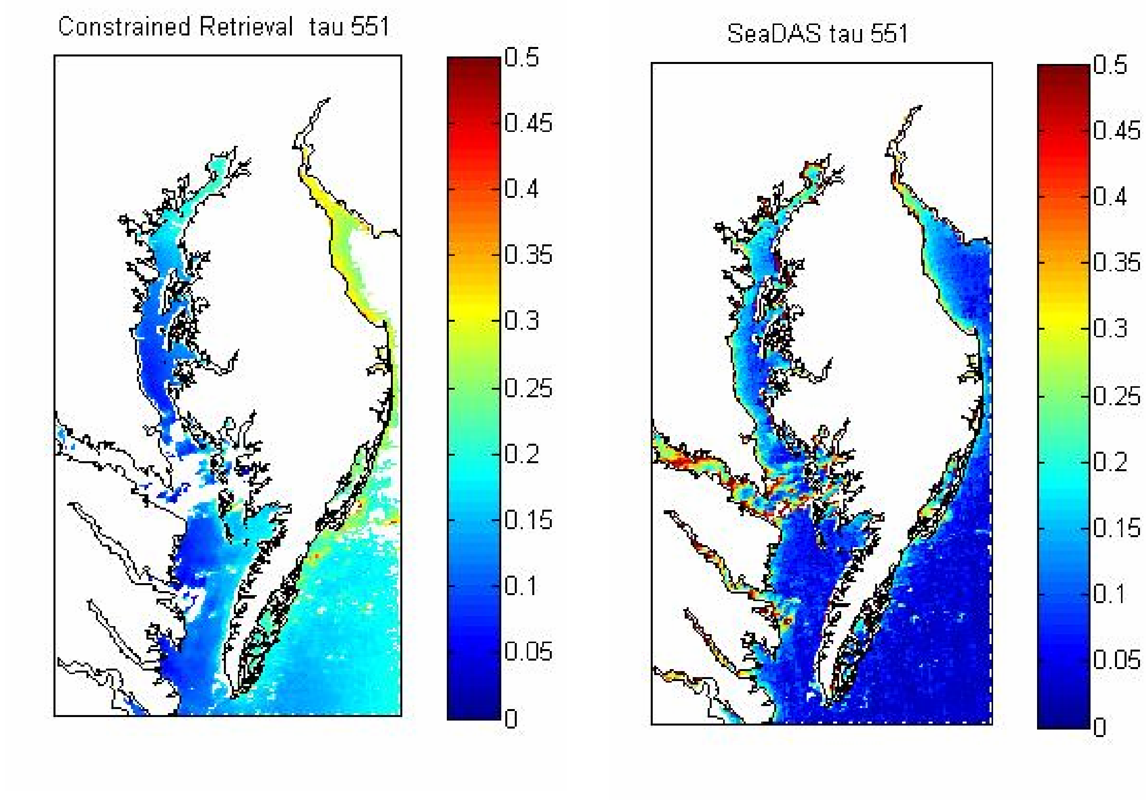

Fig. 18. Aerosol Optical Depth comparisons at 551 nm a) constrained retrieval b) SeaDAS retrieval

Table 1 Parameters and ranges used In Radiative Transfer LUT

Variable name	**Symbol**	**Range**
Wavelength	λ	(400:10:900,1240,1650,2130)
Sensor viewing angle	θ_V	(0,15,30,45,60)
Solar angle	θ_S	(0,15,30,45,60)
Azimuth	φ	(0,45,90,180)
Aerosol optical thickness	τ	(0.05:0.05:0.5

Table 2 MODIS Noise Equivalent Delta Reflectance NE$\Delta\rho$ for a solar angle of 60 degrees

Band	Wavelength [nm]	NE$\Delta\rho$
8	412	1.818×10^{-4}
9	443	1.019×10^{-4}
10	488	8.10×10^{-5}
11	531	6.01×10^{-5}
12	551	6.38×10^{-5}
13	667	3.39×10^{-5}
14	678	2.93×10^{-5}
15	748	4.63×10^{-5}
16	869	4.08×10^{-5}
5	1240	5.069×10^{-4}
6	1650	3.618×10^{-4}
7	2130	2.967×10^{-4}

Table 3 Fractional Normalized water leaving reflectance uncertainties

Atmospheric Correction		Constraint used	Uncertainty %		
Atmospheric Correction Method	Atmospheric LUT's used		Band 443nm	Band 488nm	Band 551nm
Traditional NIR	SeaDAS	10% Bright pixel compensation	25%	13%	4%
Traditional NIR	SeaDAS plus Aeronet	10% Bright pixel compensation	120%	50%	10%
SWIR	SeaDAS	No constraint at 412nm	20%	10%	3%
SWIR	SeaDAS	$2\sigma\ \rho_{wn}(412)$ $\rho_{wn}(412) = .005 \pm .005$	20%	10%	3%
SWIR	SeaDAS	$1\sigma\ \rho_{wn}(412)$ $\rho_{wn}(412) = .005 \pm .003$	18%	8%	3%
SWIR	SeaDAS plus Aeronet	No constraint at 412nm	90%	35%	10%
SWIR	SeaDAS plus Aeronet	$2\sigma\ \rho_{wn}(412)$ $\rho_{wn}(412) = .005 \pm .005$	40%	15%	5%
SWIR	SeaDAS plus Aeronet	$1\sigma\ \rho_{wn}(412)$ $\rho_{wn}(412) = .005 \pm .003$	15%	8%	3%

Table 4 Matchups of insitu Remote Sensing Reflectance and SeaDAS retrievals from MODIS TERRA satellite including both NIR and SWIR atmosphere correction methods.

					in situ Rrs values		satellite Rrs values (SeaDAS)			
#	Date	Time	Lat.	Long	Rrs412	Rrs443	NIR Rrs412	NIR Rrs443	SWIR Rrs412	SWIR Rrs443
1	19-Jul-02	18:35:00	37.92	-76.19	4.88E-04	7.65E-04			1.39E-04	2.46E-04
2	2-Oct-02	16:50:00	39.25	-76.24	9.52E-04	1.66E-03			-4.70E-04	-5.60E-04
3	2-Oct-02	18:47:00	39.00	-76.36	3.20E-04	4.92E-04			-2.52E-03	-1.97E-03
4	2-Oct-02	20:25:00	38.80	-76.45	4.03E-04	5.25E-04	-7.50E-04	-1.90E-04	8.50E-04	1.39E-03
5	31-Mar-03	14:50:00	39.34	-76.18	2.24E-04	5.88E-04			-6.93E-05	-4.75E-05
6	31-Mar-03	19:30:00	39.00	-76.37	1.49E-04	5.61E-04			1.90E-03	3.13E-03
7	31-Mar-03	21:10:00	38.80	-76.44	2.95E-04	7.66E-04	-2.58E-03	-1.49E-03	-2.41E-03	-1.18E-03
8	3-Oct-03	13:28:00	37.27	-76.15	1.54E-03	2.17E-03	-1.71E-03	-2.70E-04	7.20E-04	1.74E-03
9	3-Oct-03	16:31:00	37.58	-76.17	1.11E-03	1.64E-03	-1.67E-03	-7.30E-04	-3.29E-03	-2.48E-03
10	3-Oct-03	22:15:00	38.26	-76.34	5.09E-04	1.04E-03	-4.54E-03	-2.60E-03	-6.11E-03	-4.24E-03
11	27-May05	15:40:00	36.91	-75.94	2.71E-03	3.43E-03	2.52E-03	3.05E-03	6.28E-03	6.91E-03
12	27-May05	17:40:00	36.84	-75.88	3.24E-03	4.53E-03	1.44E-03	1.98E-03	5.76E-03	6.43E-03
13	27-May05	19:09:00	36.83	-75.82	2.69E-03	3.69E-03	3.05E-03	3.84E-03	8.91E-03	9.55E-03
14	27-May05	19:26:00	36.86	-75.78	2.89E-03	3.88E-03	3.61E-03	4.44E-03	9.36E-03	1.01E-02
15	26-Jul-05	13:32:00	37.48	-75.53	2.39E-03	3.06E-03			1.22E-02	1.27E-02
16	26-Jul-05	15:49:00	37.17	-75.39	2.51E-03	2.80E-03	2.81E-03	2.84E-03	1.22E-02	1.16E-02
17	26-Jul-05	18:33:00	37.09	-75.71	2.27E-03	2.87E-03	5.00E-04	5.90E-04	1.25E-02	1.26E-02